Coarsening dynamics in a two-species zero-range process

S. Großkinsky[1] and T. Hanney[2]
[1]*Zentrum Mathematik, Technische Universität München, 85747 Garching bei München, Germany*
[2]*School of Physics, University of Edinburgh, Mayfield Road, Edinburgh EH9 3JZ, United Kingdom*
(Received 21 December 2004; revised manuscript received 1 April 2005; published 29 July 2005)

We consider a zero-range process with two species of interacting particles. The steady-state phase diagram of this model shows a variety of condensate phases in which a single site contains a finite fraction of all the particles in the system. Starting from a homogeneous initial distribution, we study the coarsening dynamics in each of these condensate phases, which is expected to follow a scaling law. Random-walk arguments are used to predict the coarsening exponents in each condensate phase. They are shown to depend on the form of the hop rates and on the symmetry of the hopping dynamics. The analytic predictions are found to be in good agreement with the results of Monte Carlo simulations.

DOI: 10.1103/PhysRevE.72.016129 PACS number(s): 02.50.Ey, 64.60.−i, 64.75.+g

I. INTRODUCTION

Since the first observation of a condensation transition in the homogeneous zero-range process (ZRP) [1], there has been a lot of activity to further study this phenomenon on the level of the steady state [2], and on the level of the relaxation dynamics [2,3]. When the density of particles exceeds a critical value, the system has been shown to phase separate into a homogeneous background and a condensate which contains a finite fraction of all the particles in the system. In the steady state, the condensate occupies only a single lattice site, and starting with homogeneous initial conditions, the relaxation dynamics exhibit an interesting coarsening phenomenon.

Besides being of interest in its own right as an example of a condensation transition in an exactly solvable model, the phenomenon is relevant in a more general context, providing a criterion for phase separation in driven diffusive systems [4,5]. The basic condensation mechanism is by now well understood on a static and dynamic level, but generalizations continue to be a topic of current interest, such as coarsening behavior on scale-free networks [6], processes with defect sites [7], or applications to bipartite graphs [8]. Of particular interest are generalizations to two-species zero-range processes with two conservation laws, which also exhibit condensation and have a much richer stationary phase diagram than that of the single-species system [9,10]. Indeed, while the stationary and dynamical properties of one-dimensional driven diffusive systems with one species of particles are relatively well understood, much less is known about the properties, and in particular the dynamical properties, of driven systems with two or more species of conserved particles (see [11] for a recent review).

This paper provides an analysis of the coarsening dynamics of a two-species zero-range process. We generalize the arguments in [2] for a single-species system, which turns out to be far from straightforward since several new effects have to be taken into account, effects due to the coupled dynamics of the two-particle species. The model is chosen such that all the expected new features can be observed while the steady state is exactly solvable. In addition to this theoretical interest, the results are relevant for physical realisations of two-species zero-range processes, which can be found, for example, in shaken bidisperse granular systems [12] and models of directed networks [13].

In Sec. II, we define the model which is a generalization of the model considered in [10], recap some known results for the steady state, and give the phase diagram. In Sec. III, we state the expected scaling behavior for the coarsening regime and explain the random-walk arguments for its analysis. The main results of the paper are derived in Sec. IV, namely scaling laws for the time evolution of the mean condensate size for all regions of the phase diagram, generalizing the derivation in [2]. The predictions are compared to Monte Carlo simulation data and we find good agreement. We conclude in Sec. V and include a discussion of finite-size effects in an Appendix.

II. MODEL

A. Definition and steady state

We define the two-species zero-range process on a one-dimensional lattice containing L sites with periodic boundary conditions. On this lattice, there are N_1 particles of species 1 and N_2 particles of species 2. A site with occupation numbers k_1 and k_2 for species 1 and 2, respectively, loses a particle of species 1 with rate $g_1(k_1,k_2)$ and of species 2 with rate $g_2(k_1,k_2)$. For simplicity, we assume that particles hop to their nearest-neighbor site to the right, although our results also apply for more general hopping of finite range.

The steady states for this model with general $g_1(k_1,k_2)$ and $g_2(k_1,k_2)$ have been characterized in [9,14] and we now summarize the main points. We denote a particle configuration by $\mathbf{k}=k_{1,1},k_{2,1};\ldots;k_{1,L},k_{2,L}$. The steady-state probabilities assume a factorized form

$$\nu_{\mathbf{z}}^{L}(\mathbf{k}) = \prod_{x=1}^{L} \nu_{\mathbf{z}}(k_{1,x},k_{2,x}), \tag{1}$$

provided the hop rates satisfy the constraint

$$\frac{g_1(k_1,k_2)}{g_1(k_1,k_2-1)} = \frac{g_2(k_1,k_2)}{g_2(k_1-1,k_2)} \tag{2}$$

for all $k_1,k_2 \geqslant 1$. The single-site distribution has the form

$$\nu_{\mathbf{z}}(k_1,k_2) = \frac{1}{Z(\mathbf{z})} f(k_1,k_2) z_1^{k_1} z_2^{k_2}, \tag{3}$$

where $f(k_1,k_2)$ is a stationary weight which can be written

$$f(k_1,k_2) = \prod_{i=1}^{k_1} \frac{1}{g_1(i,0)} \prod_{j=1}^{k_2} \frac{1}{g_2(k_1,j)}. \tag{4}$$

Here $\mathbf{z}=(z_1,z_2)$, $z_i \geqslant 0$ play the role of fugacities for each species, in that they are chosen to fix the particle densities $\rho_i = \langle N_i \rangle_\nu / L$ for species $i=1,2$, i.e., the expected number of particles per site in the steady state. Thus we are working in a grand canonical ensemble, which is normalized by the single-site partition function $Z(\mathbf{z})$. This steady state can be directly obtained by substitution into the balance condition for the steady-state probability that the system is in a configuration $\mathbf{k}$.

We remark that one gets the same steady state if the hopping dynamics are symmetric, rather than asymmetric as defined above. A useful property of the steady state [9,14] is that the expectation value of the hop rate of species i, denoted by $\langle g_i \rangle_\nu$, is equal to z_i. Thus $\langle g_i \rangle_\nu$ is a translation invariant quantity; this is obvious in the case of asymmetric dynamics, where $\langle g_i \rangle_\nu$ is the current, but less obvious in the case of symmetric dynamics with vanishing current, where $\langle g_i \rangle_\nu > 0$.

We are interested in the coarsening dynamics of the model in various phases that arise for a particular choice of rates, namely

$$g_1(k_1,k_2) = \left(\frac{1 + b/(k_1+1)^\gamma}{1 + b/k_1^\gamma} \right)^{k_2} (1 + c/k_1),$$

$$g_2(k_1,k_2) = 1 + b/(k_1+1)^\gamma, \tag{5}$$

where $g_1(0,k_2) = g_2(k_1,0) = 0$ and $b,c,\gamma > 0$. It is easy to check by substitution that these rates satisfy the constraint (2). The stationary weights, obtained from Eq. (4), are given by

$$f(k_1,k_2) = \frac{k_1!}{(1+c)_{k_1}} \left(1 + \frac{b}{(k_1+1)^\gamma} \right)^{-k_2}, \tag{6}$$

where $(a)_k = \prod_{i=0}^{k-1} (a+i)$ is the Pochhammer symbol. The single-site partition function is given by

$$Z(\mathbf{z}) = \sum_{k_1,k_2=0}^{\infty} f(k_1,k_2) z_1^{k_1} z_2^{k_2}$$

$$= \sum_{k_1=0}^{\infty} z_1^{k_1} \frac{(k_1+1)^\gamma + b}{(1-z_2)(k_1+1)^\gamma + b} \frac{k_1!}{(1+c)_{k_1}}. \tag{7}$$

We make the choice (5) in order to study the behavior when the dynamics of one of the particle species, here species 2, depends only on the number of particles of the other species at the departure site. So condensation of species 2, when it occurs, is induced by the presence of species 1 particles, which can be interpreted as an evolving disordered background as discussed for a specific case in Sec. IV C. The k_2 dependence in g_1 is then determined by the constraint (2). The second factor $(1+c/k_1)$ in g_1 could be replaced by any function of k_1 and the steady state will still factorize. The form we have chosen is the simplest form of the hop rate for which the single-species zero-range process exhibits a condensation transition for $c>2$ at a finite critical density of particles [1]. Thus the parameter c can be tuned to allow also condensation of species 1 particles, which influences the phase diagram of the process as discussed in Sec. II B. We remark that the existence of condensation transitions and any subsequent coarsening behavior depend only on the asymptotic forms of the rates. Other choices of this second factor, with different asymptotic properties, lead either to no transition of species 1 particles if it is nondecreasing or tends to a constant faster than $2/k_1$ as $k_1 \to \infty$, or to condensation at any density (where the fraction of particles in the condensate is equal to 1) if it tends to zero as $k_1 \to \infty$. Thus Eqs. (5) are basic rates which capture two different mechanisms of condensation transition (i.e., induced and autonomous) and the most interesting coarsening behavior that we expect to observe while the steady state remains exactly solvable.

B. Stationary phase diagram

The range of possible fugacities is given by the domain of convergence of the partition function $Z(\mathbf{z})$ given in Eq. (7). In the present case, the maximal fugacities are $z_1=1$ and $z_2=1$, and when one or both of the fugacities are maximal we use the notation $\mathbf{z}=\mathbf{z}_c$. The phase diagram in terms of the particle densities ρ_1 and ρ_2 has been derived in [10,15]. For the grand canonical ensemble (3), the densities are given by

$$\rho_i = z_i \frac{\partial \ln Z(\mathbf{z})}{\partial z_i}, \quad i=1,2, \tag{8}$$

and thus the convergence properties of the partition function at the maximal fugacities determine whether the critical densities $\rho_{i,c} := \rho_i|_{z_i=1}$ are finite or infinite. In general, $\rho_{1,c}$ can depend on ρ_2, i.e., $\rho_{1,c} = \rho_{1,c}(\rho_2)$ and vice versa. If $\rho_i \leqslant \rho_{i,c}$ for $i=1,2$, both species are in a fluid phase corresponding to a factorized steady state $\nu_{\mathbf{z}}$ as given in Eq. (3). In the phase diagram shown in Fig. 1, this region is denoted by D. If the particle density ρ_i of either species $i=1,2$ exceeds its critical value $\rho_{i,c}$, species i condenses: the system phase separates into a homogeneous background fluid phase with distribution $\nu_{\mathbf{z}_c}$ and a condensate which contains the $(\rho_i - \rho_{i,c})L$ "excess" particles of species i. In a typical stationary configuration this condensate occupies a single, randomly located site.

Depending on the values of c and γ in Eq. (5) the following phases appear in the phase diagram in addition to the fluid phase D.

(i) In region A, the fugacities are $\mathbf{z}_c=(1,z_2)$ with $z_2<1$. The species 1 particles condense and the species 2 particles form a fluid. The particle densities in the background phase are $(\rho_{1,c},\rho_2)$.

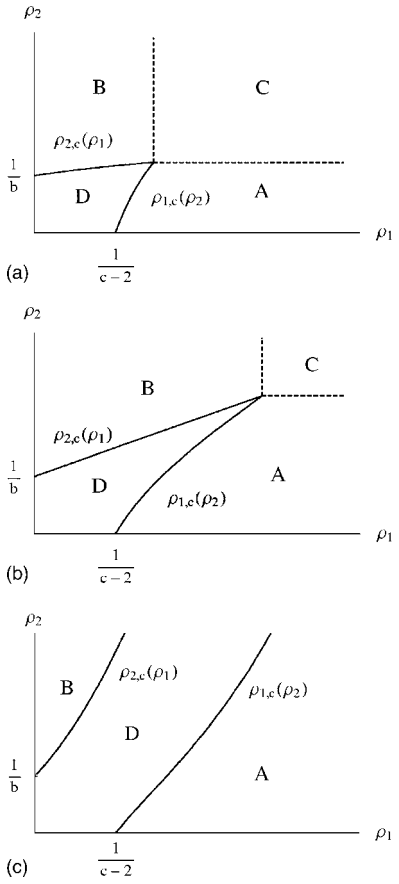

FIG. 1. Phase diagram for the choice of rates (5) with $b=1$, $c=4$, and several values of γ. For $\gamma=0.5$ (a) and $\gamma=1$ (b) it is $c>\max(2+\gamma,1+2\gamma)$ and region C exists, whereas for $\gamma=2$ (c) we have $c<\max(2+\gamma,1+2\gamma)$ and region C does not exist. See text for details.

(ii) In region B, the fugacities are $\mathbf{z}_c=(z_1,1)$ with $z_1<1$, species 2 condenses, and the background particle densities are $(\rho_1,\rho_{2,c})$. As an additional point, the site containing the condensate of species 2 particles also contains $O(L^{1/(1+\gamma)})$ species 1 particles [9].

(iii) In region C, $\mathbf{z}_c=(1,1)$. A single site contains condensates of both species and the background densities are $(\rho_{1,c},\rho_{2,c})$.

The phase diagram shown in Fig. 1 is richest when $c>\max(2+\gamma,1+2\gamma)$, where all three regions are found. For $2<c\leqslant\max(2+\gamma,1+2\gamma)$, the phase diagram contains only the phases A, B, and D, and for $c\leqslant 2$ only phases B and D remain.

So far we have discussed straightforward generalizations of previously known results. We now turn to the main aim of this work, which is to study the coarsening dynamics of the two-species zero-range process leading to each of the condensate phases A, B, and C.

III. COARSENING

In the following, we use the symbol $\approx$ to denote asymptotic expansions in the thermodynamic limit $L\to\infty$ with fixed particle densities, i.e., $N_1=[\rho_1 L]$ and $N_2=[\rho_2 L]$. If the terms in the expansion are only given up to a constant factor, we use the symbol $\sim$ instead.

A. Relaxation dynamics

In this section, we outline the arguments used to describe the coarsening dynamics in the condensate phases. Starting from an initially uniform distribution of particles, the dynamics of the condensation can be divided into three regimes.

(i) Nucleation, during which excess particles of either species accumulate at several randomly located sites, which we call *cluster sites*. Each contains $O(L)$ particles, so there are $O(1)$ cluster sites, separated by a typical distance of order L. At the remaining sites, which we call *bulk sites*, the system relaxes to its steady-state distribution $\nu_{\mathbf{z}_c}$.

(ii) Coarsening, during which the cluster sites exchange particles through the bulk. This leads to the growth of large condensates at the expense of smaller ones and a decrease in the number of cluster sites.

(iii) Saturation, where eventually only two cluster sites remain due to the finite size of the system. In this regime the dynamics, under which the system reaches a typical steady-state configuration with a single cluster site, is different from the coarsening dynamics (cf. [2]).

Physically, the most interesting is the coarsening regime. Here, large condensates gain particles at the expense of smaller ones, which causes some condensates to disappear. This in turn leads to a decrease in the number of cluster sites and hence an increase of the mean condensate size $m_i(t)$, defined as the number of particles of species $i=1,2$ at cluster sites divided by the number of cluster sites at time t. In the limit $t\to\infty$, $m_i(t)$ converges to its steady-state value $(\rho_i-\rho_{i,c})L$, the number of excess particles of species i in the system. Within the coarsening regime, the increase of the mean condensate size is expected to follow a scaling law, $\langle m_i(t)\rangle_L\sim t^{\beta_i}$. Moreover, on a certain time scale $\tau=\tau(L)$, the growth of the normalized mean condensate size is expected to be independent of the system size L,

$$\frac{\langle m_i(t)\rangle_L}{(\rho_i-\rho_{i,c})L}\sim(t/\tau)^{\beta_i}. \tag{9}$$

Therefore, the scale L of the mean condensate size and the time scale τ are connected via $L\sim\tau^{\beta_i}$, and thus $\tau\sim L^{1/\beta_i}$. The angled brackets $\langle\cdots\rangle_L$ denote an ensemble average in a finite system of size L, starting with a homogeneous distribution of $N_j=[\rho_j L]$ particles for both species $j=1,2$. This is in contrast to the steady-state expectation denoted by $\langle\cdots\rangle_\nu$. The scaling law (9) defines the exponent β_i, which may depend on the particle species i. In general, one could choose different observables to monitor the coarsening process, such as the square sum of occupation numbers. But in our case the mean condensate size is a natural choice, since it is directly accessible by our arguments given below.

We remark that the scaling law (9) is of the same form as that which describes the growth of characteristic length scales in phase-ordering dynamics [16]. More precisely, one can define a scaling function

$$h_i(t') := \lim_{L\to\infty} \frac{\langle m_i(t'\tau)\rangle_L}{(\rho_i-\rho_{i,c})L} \tag{10}$$

for all $t' \geqslant 0$. With the appropriate time scale τ, which will be derived in the next section for the various phases, h_i is expected to be a nondegenerate, smoothly increasing function with the asymptotic properties

$$h_i(t') = O(t'^{\beta_i}) \quad \text{for } t' \to 0 \quad \text{and} \quad \lim_{t'\to\infty} h_i(t') = 1. \tag{11}$$

So for small t', the coarsening regime is described by a power law (9) which we study in the following. For $t' \to \infty$, the system saturates and h_i converges to its maximal value 1. We do not discuss further the behavior in this regime; this has been done for a single-species system in [2].

B. Random-walk arguments

In the following, our aim is to estimate the exponents β_i in each of the condensate phases A, B, and C of the model defined by the rates (5). This is achieved by adapting the random-walk arguments given for the coarsening dynamics of the one-species model [2]. They are based on two major assumptions, which are self-consistent and confirmed by simulation data.

(A1) *Separation of time scales*. The nucleation process is very fast so that during the coarsening regime the bulk sites have already relaxed to the steady state distribution $\nu_{\mathbf{z}_c}$.

Within the coarsening regime, the system can therefore be separated into a stationary bulk and a finite number of isolated cluster sites. On top of stationary hop rates $\langle g_i\rangle_\nu = z_{i,c}$, cluster sites of species i exchange particles through the bulk on a slower time scale, given below. The bulk can be seen as a homogeneous medium through which these excess particles perform a biased random walk, and the cluster sites as boundaries where they enter and exit.

(A2) *Independence of excess particles in the bulk*. The excess particles exchanged by cluster sites perform independent (biased) random walks through the bulk on their way to the next cluster site and do not effect the bulk distribution $\nu_{\mathbf{z}_c}$.

This is justified below by noting that the average density of excess particles in the bulk vanishes for $L \to \infty$.

The random-walk argument then proceeds as follows. We consider the case where one species $i=1$ or 2 condenses. The rates we consider decay as $g_i - 1 \sim k_i^{-\alpha}$ with $0 < \alpha \leqslant 1$ (see Sec. IV) and the average hop rate in the bulk is $z_{i,c}=1$. So the effective rate at which cluster sites with $k_i \sim L$ lose particles to the bulk is $g_i - z_{i,c} \sim L^{-\alpha}$. These excess particles perform a biased random walk through the bulk with drift,

$$\langle g_i | k_i > 0\rangle_\nu - \langle g_i\rangle_\nu = \frac{\langle g_i\rangle_\nu}{1-\nu_{\mathbf{z}_c}(k_i=0)} - \langle g_i\rangle_\nu = \frac{1}{1-\nu_{\mathbf{z}_c}(k_i=0)} - 1. \tag{12}$$

Since $\nu_{\mathbf{z}_c}(k_i=0) > 0$, this is positive and independent of L. Thus the time it takes an excess particle to reach a neighboring cluster site scales as the typical distance between cluster sites, which is $O(L)$. So n independent excess particles exit the bulk with rate $O(n/L)$, which has to balance the entry rate of order $L^{-\alpha}$. Hence, the number of excess particles in the bulk scales as $O(L^{1-\alpha})$, which grows only sublinearly with L for $0 < \alpha \leqslant 1$, consistent with (A2).

In this balanced situation, the time scale on which cluster sites exchange single particles through the bulk is $O(L^\alpha)$. The time scale on which cluster sites exchange a finite fraction $\sim L$ of their particles is thus $O(L^{1+\alpha})$. Since by definition the number of cluster sites during coarsening is of order 1, this sets the coarsening time scale τ and the coarsening exponent β_i in Eq. (9) to be

$$\tau \sim L^{1+\alpha}, \quad \beta_i = \frac{1}{1+\alpha}. \tag{13}$$

With the above considerations, we can give an additional motivation for the scaling behavior (9). We have seen that the rate at which cluster sites exchange particles through the bulk depends on their size as $k_i^{-\alpha}$. Thus, in a very rough approximation, the time derivative of the average condensate size $\langle m_i(t)\rangle_L$ should be proportional to the average exchange rate of excess particles,

$$\frac{d\langle m_i(t)\rangle_L}{dt} \sim \langle m_i(t)\rangle_L^{-\alpha}. \tag{14}$$

As the solution, we recover the scaling law (9) with exponent β_i as given above. This is of course not a strict argument and should not be understood as a derivation of the scaling law.

Compared to the bulk dynamics, the coarsening is a very slow process and typical configurations with cluster sites on top of a stationary background are quasistationary, i.e., within times of order 1 the configurations at cluster sites do not change on average. To leading order in L, the dynamics on cluster sites have to be compatible with the stationary bulk dynamics. By compatibility we mean that the translation invariance of $\langle g_i\rangle_\nu$ implies that it must be the same for all sites (both cluster sites and bulk sites) in the system. For two-component systems, this induces consistency relations between the occupation numbers k_1 and k_2 on cluster sites, a fact that will often be used below. If these relations are not fulfilled, the configuration is not quasistationary in the above sense and changes on time scales of order 1 through interaction with the bulk.

IV. COARSENING SCALING LAWS

A. Theoretical predictions

We now apply the arguments described above to the model at hand and explain additional effects due to the presence of two species of particles.

1. Phase A

In phase A, $\rho_1 > \rho_{1,c}$ and only the first species condenses. There are $(\rho_1 - \rho_{1,c})L$ excess particles of species 1 in the system and at the cluster sites $k_1 = O((\rho_1-\rho_{1,c})L)$, while k_2 re-

mains finite in the limit $L\to\infty$, which is justified below by compatibility with the bulk. Hence, at the cluster sites the rates (5), up to first order in k_1, are given by

$$g_1(k_1,k_2)\approx 1+c/k_1,\quad g_2(k_1,k_2)\approx 1+b/k_1^{\gamma}. \tag{15}$$

Thus the coarsening of the species 1 particles is independent of the second species: the net rate at which particles leave a cluster site is $g_1-1=c/k_1$. Following the arguments leading to Eq. (13) in Sec. III B, the coarsening time scale is thus

$$\tau_A\sim[(\rho_1-\rho_{1,c})L]^2, \tag{16}$$

and we expect that the normalized mean condensate size grows like

$$\frac{\langle m_1(t)\rangle_L}{(\rho_1-\rho_{1,c})L}\sim(t/\tau_A)^{1/2},\quad \text{i.e.,}\quad \beta_1=1/2. \tag{17}$$

This recovers the known coarsening of the condensate in the one-species ZRP where particles hop with rate $1+c/k$ [2,3].

Further, because the jump rates of both species are coupled, the presence of a species 1 condensate influences the distribution P of the species 2 particles on the cluster site: Since cluster sites and bulk have to be compatible, g_2 on the cluster site has to be equal to the bulk steady-state current $\langle g_2\rangle_\nu=z_2<1$, and using Eq. (15) we have

$$\langle g_2\rangle_\nu\approx(1+b/k_1^{\gamma})P(k_2>0)\approx P(k_2>0). \tag{18}$$

Therefore, $P(k_2=0)\approx 1-\langle g_2\rangle_\nu$. This is nonzero, but smaller than the expected bulk value, which contains an extra positive contribution due to $b/k_1^{\gamma}=O(1)$.

2. Phase B

In phase B, $\rho_2>\rho_{2,c}$ and the second species condenses. The number of particles at a cluster site is $k_2=O((\rho_2-\rho_{2,c})L)$. Now, using Eq. (5), the hop rate g_1 of the first species at a cluster site vanishes in the limit $L\to\infty$ if $k_1=O(1)$. But since in the bulk the mean hop rate of the first species is given by its steady-state value $\langle g_1\rangle_\nu=z_1\in(0,1)$ for $\rho_1>0$, k_1 has to be large at cluster sites. Thus, considering k_1 large in Eq. (5), the hop rate of species 1 particles at cluster sites becomes

$$g_1(k_1,k_2)\approx\exp(-b\gamma k_2/k_1^{1+\gamma})(1+c/k_1), \tag{19}$$

which should be consistent with the expected bulk value $\langle g_1\rangle_\nu=z_1$. This compatibility requirement leads to

$$k_1^{1+\gamma}\approx -b\gamma k_2/\ln z_1, \tag{20}$$

and this relation between k_1 and k_2 is dynamically stable since on cluster sites

$$\partial_{k_1}[g_1(k_1,k_2)-z_1]\big|_{k_1^{1+\gamma}\approx -b\gamma k_2/\ln z_1}\approx\frac{-(1+\gamma)z_1\log z_1}{k_1}>0. \tag{21}$$

So cluster sites where k_1 is too small gain species 1 particles from the bulk (or if k_1 is too high they are lost to the bulk), and thus any perturbation of the relationship (20) is driven toward this stable form on intermediate time scales. Hence cluster sites at which Eq. (20) is satisfied dominate the coarsening, and the hop rate of the second species can be written

$$g_2(k_1,k_2)=1+b/(k_1+1)^{\gamma}\approx 1+\left(\frac{-b^{1/\gamma}\ln z_1}{\gamma k_2}\right)^{\gamma/(1+\gamma)}. \tag{22}$$

Therefore, particles of species 2 escape from a cluster site at a net rate proportional to $1/k_2^{\gamma/(1+\gamma)}$ and we can repeat the arguments given in Sec. III B to deduce the coarsening time scale

$$\tau_B\sim[(\rho_2-\rho_{2,c})L]^{(1+2\gamma)/(1+\gamma)}. \tag{23}$$

The normalized mean condensate size grows like

$$\frac{\langle m_2(t)\rangle_L}{(\rho_2-\rho_{2,c})L}\sim(t/\tau_B)^{(1+\gamma)/(1+2\gamma)},\quad \text{i.e.,}\quad \beta_2=\frac{1+\gamma}{1+2\gamma}. \tag{24}$$

3. Phase C

In phase C, $\rho_1>\rho_{1,c}$ and $\rho_2>\rho_{2,c}$ and both species condense. While in phases A and B the relationship between the occupation numbers k_1 and k_2 was fixed by compatibility with the bulk dynamics, in phase C this relationship is not uniquely determined. Using the expansion

$$g_1(k_1,k_2)\approx 1-b\gamma k_2/k_1^{1+\gamma}+c/k_1,\quad g_2(k_1,k_2)\approx 1+b/k_1^{\gamma}, \tag{25}$$

we see that for $k_1=O(L)$ any value of k_2 in the range $O(1)\leqslant k_2\leqslant O(L)$, and for $k_2=O(L)$ any value of k_1 in the range $O(L^{1/(1+\gamma)})<k_1\leqslant O(L)$, lead to $g_1\approx g_2\approx 1$ and are compatible with the bulk dynamics. All compatible relations between k_1 and k_2 may be observed during the coarsening regime, but the sites with the longest lived relation will determine the coarsening time scale.

Since the leading order of k_1 in the hop rate g_1 given in Eq. (25) depends on γ, we have to distinguish three cases.

(i) $\gamma<1$. In this case the longest lived relation is given by double cluster sites, i.e., sites with $k_1\sim k_2\sim L$. Since $g_1-1=-b\gamma k_2/k_1^{\gamma+1}<0$, such cluster sites gain excess species 1 particles from the bulk rather than losing them.

Double cluster sites are stable compared to cluster sites with other relationships between k_1 and k_2, in the sense that such sites are driven toward $k_1\sim k_2\sim L$: For $k_2=O(L)$ and $O(L^{1/(1+\gamma)})<k_1<O(L)$, one has $g_1(k_1,L)-g_1(L,L)\sim -b\gamma L/k_1^{1+\gamma}$. Therefore, the smaller the value of k_1 at cluster sites, the greater the rate at which species 1 particles are gained from the bulk. Thus k_1 is driven toward a value $O(L)$. On the other hand, for $k_1=O(L)$ and $k_2<O(L)$ one has $g_1(L,k_2)-g_1(L,L)\sim b\gamma/L^{\gamma}>0$, so cluster sites at which only $k_1=O(L)$ lose species 1 particles to double cluster sites.

Since on double cluster sites both species exchange particles with the bulk at an effective rate proportional to $1/k_i^{\gamma}$, $i=1,2$, the coarsening time scale is given by $t(k_i)\sim k_i k_i^{\gamma}$. Thus $\tau_C\sim L^{1+\gamma}$ and both species coarsen with the same exponent $\beta_i=1/(1+\gamma)$, i.e.,

$$\frac{\langle m_1(t)\rangle_L}{(\rho_1-\rho_{1,c})L} \sim \frac{\langle m_2(t)\rangle_L}{(\rho_2-\rho_{2,c})L} \sim (t/\tau_C)^{1/(1+\gamma)}. \quad (26)$$

(ii) $\gamma=1$. The longest lived sites are again double cluster sites, at which $k_1 \sim k_2 \sim L$. Now the sign of $g_1-1 \approx -b\gamma/L + c/L$ depends on b and c, but all the arguments for $\gamma<1$ apply in this case also, so we expect that the scaling law (26) still holds for $\gamma=1$.

(iii) $\gamma>1$. Now the leading order for cluster sites of the first species changes to $g_1 \approx 1+c/k_1$ independent of γ and k_2. Thus species 1 coarsens independently of species 2 with the dynamics determined in the same way as phase A, therefore $\beta_1=1/2$. However, the relation between k_1 and k_2 is not stable on cluster sites at which $k_1=O(L)$ for any value of k_2, since $g_2-1 \approx b/k_1^{\gamma} < g_1-1 \approx c/k_1$. But when k_1 is large, k_2 is driven toward large values (since g_2-1 is small), thus excess species 2 particles accumulate at sites where $k_1=O(L)$.

On species 2 cluster sites, i.e., sites where $k_2 \sim L$, the slowest time scale in the dynamics of the species 2 particles is set when the cluster site contains $k_1=O(L)$ species 1 particles. However, since the effective exit rates, g_1-1 and g_2-1, differ for each species, the coarsening mechanism is more complicated than in previous cases. This can be seen as follows. When $k_1=O(L)$, species 2 particles are lost to the bulk with an effective rate proportional to $O(L^{-\gamma})$. Now, the time it would take for $O(L)$ species 2 particles to escape to the bulk scales as $O(L^{1+\gamma})$, which is large (since $\gamma>1$) compared to the time scale $O(L^2)$ over which the species 1 particles coarsen. Therefore, after a time of order $O(L^2)$, the number of species 2 particles at a cluster site is still $O(L)$ but the number of species 1 particles has decreased to its minimum value allowed by continuity, $O(L^{1/(1+\gamma)})$. Now the species 2 particles are lost to the bulk in a time of order $O(L^{1+\gamma/(1+\gamma)})$ which is fast relative to the time of order $O(L^2)$ we have already waited for the species 1 particles to coarsen. Thus the species 2 cluster dismantles immediately following the dissolution of the species 1 cluster. Hence both species coarsen on a time scale $\tau_C \sim L^2$ and we expect

$$\frac{\langle m_1(t)\rangle_L}{(\rho_1-\rho_{1,c})L} \sim \frac{\langle m_2(t)\rangle_L}{(\rho_2-\rho_{2,c})L} \sim (t/\tau_C)^{1/2}. \quad (27)$$

The coarsening of species 2 almost exclusively takes place on vanishing species 1 cluster sites. In this sense, the coarsening of the species 2 particles is effectively a slave to that of the species 1 particles. Indeed in simulations this picture is confirmed, and both species coarsen on the same time scale, but the species 1 particles coarsen first (see Fig. 4 in the next section).

The results for each phase are summarized in Table I. These theoretical predictions are compared with numerical results, which are presented in the next subsection, in Fig. 2.

TABLE I. Coarsening exponents for asymmetric hopping.

Phase	Coarsening exponents
A	$\beta_1=1/2$
B	$\beta_2=(1+\gamma)/(1+2\gamma)$
C, $\gamma \leqslant 1$	$\beta_1=\beta_2=1/(1+\gamma)$
C, $\gamma>1$	$\beta_1=\beta_2=1/2$

B. Comparison to simulation data

The theoretical predictions of the previous subsection are compared to Monte Carlo simulations in Figs. 3 and 4. $N_1=[\rho_1 L]$ and $N_2=[\rho_2 L]$ particles of species 1 and 2, respectively, are initially distributed on a lattice of size L with uniform probability. Cluster sites of species i are defined by the threshold $(\rho_i-\rho_{i,c})L/40$. The proportionality factor has to be chosen such that bulk fluctuations are well separated from cluster sites. Results for exponents are not sensitive to this choice for the system sizes considered, ranging from $L=256$ to 4096, since the fluctuations grow only sublinearly in L. With this threshold we measure the mean condensate size $m_i(t)$ and other observables, such as the bulk density $\rho_{i,\mathrm{bulk}}(t)$, of species i as a function of time, scaled with the expected coarsening time scale τ. The ensemble average $\langle\cdots\rangle_L$ is approximated by averaging over 400 sample runs for each system size.

In the following, we discuss the expected behavior of the observables, which is consistent with simulation results, up to finite-size effects, discussed in the Appendix. Plots of the normalized mean condensate size $\langle m_i(t)\rangle_L/(\rho_i-\rho_{i,c})L$ for different system sizes L against the rescaled time t/τ, where τ is the predicted coarsening time scale, are expected to collapse onto a single curve. Within the coarsening regime, this curve should be described by the scaling laws derived in Sec. IV.

During nucleation, more and more particles become trapped in cluster sites, therefore the bulk density $\rho_{i,\mathrm{bulk}}(t)$ is a decreasing function of time, approaching the critical density $\rho_{i,c}$. This is used as a criterion to identify the beginning of the coarsening regime. The end of the coarsening regime is reached approximately when $\langle m_i(t)\rangle_L=0.4(\rho_i-\rho_{i,c})L$, corresponding to an average of 2.5 remaining cluster sites. For later times the data significantly deviate from the scaling law and the system saturates, as already explained in Eq. (10). Within the coarsening time regime defined above, we make a linear fit to the double logarithmic data points of the normalized mean condensate size, showing an approximately linear behavior. The measured slope gives the numerical estimate for the coarsening exponent β_i. To get sensible error estimates we slice the coarsening time window into four smaller

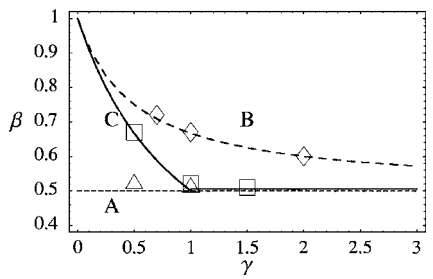

FIG. 2. Comparison of the theoretical predictions, indicated by lines, with the numerical estimates of the exponents obtained in phase A (△), B (◇), and C (□). Errors are of the size of the symbols.

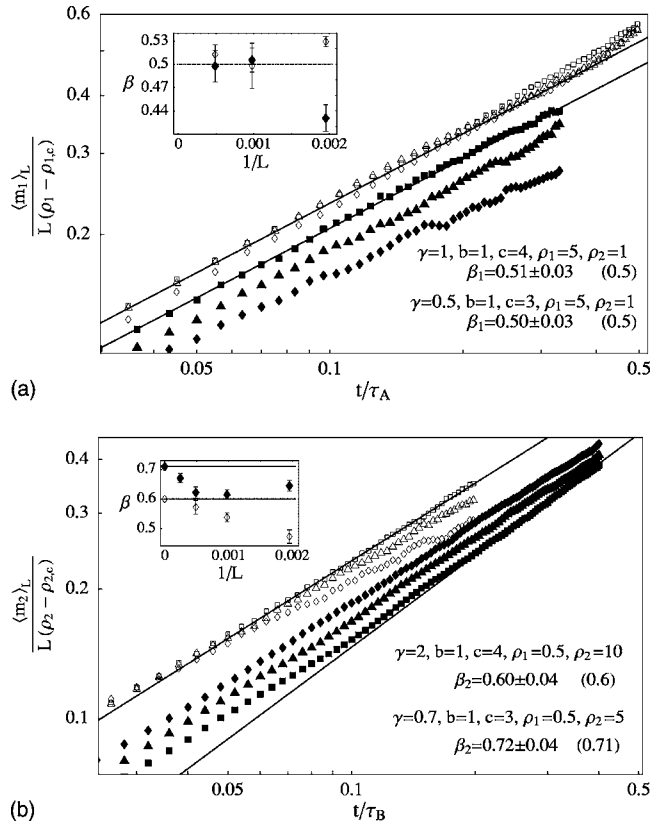

FIG. 3. Verification of the predicted scaling laws, denoted by straight lines in a double logarithmic plot of the normalized mean condensate size $\langle m_i(t)\rangle_L / L(\rho - \rho_c)$ for asymmetric hopping as a function of time. The predicted scaling exponents are given in parentheses. The insets show the finite-size scaling for the numerical estimates, where filled and unfilled symbols correspond to the data. Top: Phase A with two sets of parameters. Symbols L=512 (◇), 1024 (△), and 2048 (□) for γ=1 and filled symbols for γ=0.5. Bottom: Phase B with two sets of parameters. Symbols L=512 (◇), 1024 (△), and 2048 (□) for γ=2 and L=1024 (♦), 2048 (▲), and 4096 (■) for γ=0.7.

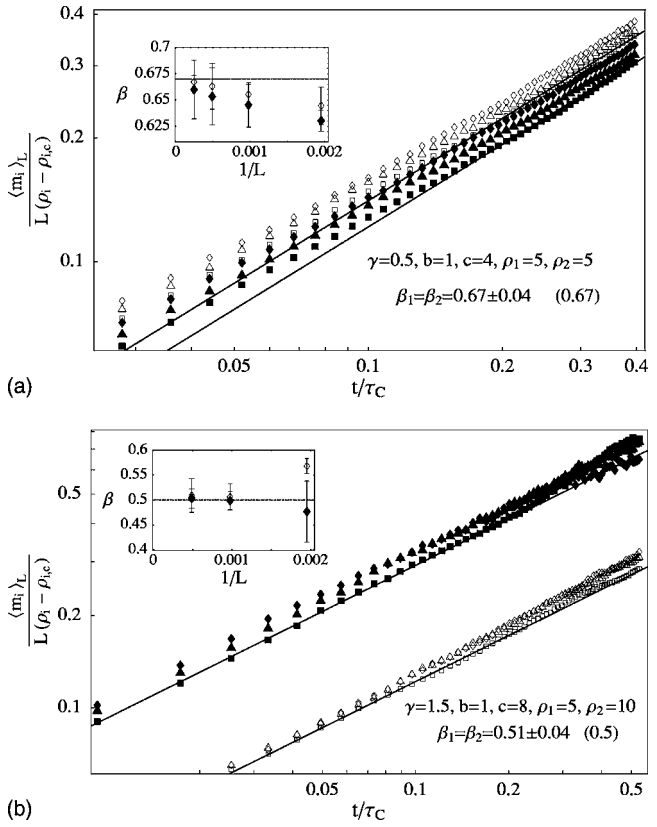

FIG. 4. Verification of the predicted scaling laws in phase C. The plots are analogous to Fig. 3, except that each one corresponds to only one value of γ and condensate sizes of both species are shown in filled and unfilled symbols. Top: Phase C with γ=0.5. Symbols L=1024 (◇), 2048 (△), and 4096 (□) for species 2 and filled symbols for species 1. Bottom: Phase C with γ=1.5. Symbols L=512 (◇), 1024 (△), and 2048 (□) for species 2 and filled symbols for species 1.

time windows (which may overlap), and measure the exponent in each of the windows. The error β_i is then taken as the standard deviation of these measurements.

The simulation results are shown in Fig. 3 for phases A and B, and in Fig. 4 for phase C. We plot the data on a double logarithmic scale for the three largest system sizes and compare to the expected scaling law given by straight lines. Finite-size scaling of the measured exponents is given in the insets. In phase C, the measurements show rather large errors but are in good agreement with the predictions. For γ=1.5 we see that, as expected, the species 1 particles coarsen first, but with the same exponent as species 2 particles. In phases A and B error bars are smaller, but there are stronger finite-size effects affecting the quality of the data collapse. Nevertheless, the measured scaling exponents are in good agreement with the predictions.

Finite-size effects strongly depend on the parameter γ, and since there are many competing mechanisms the value or even the sign of the resulting finite-size correction is very hard to estimate. We provide a discussion of these finite-size effects and their influence on the data collapse in the Appendix.

C. Discussion

One can also obtain predictions for the coarsening exponents when the hopping is symmetric. In this case, there is a high probability that a particle leaving a cluster site will return to the same site. The probability that it reaches the next cluster site is inversely proportional to the distance between cluster sites [17], so it is of order L^{-1}. Therefore, only every $O(L)$th excess particle will reach the next cluster site. Hence the coarsening time scales are increased by a factor of order L. The assumption that excess particles move independently through the bulk remains a good one, however: the time it takes particles to enter the bulk increases by a factor $O(L)$ (compared with the driven case) since most particles return to the site they have just left; this cancels the $O(L)$ increase in the time particles spend in the bulk due to the diffusive rather than driven motion. Then the arguments presented for the driven case with the extra factor $O(L)$ in the coarsening time scales lead to the exponents given in Table II. We compare the prediction to preliminary simulation data

TABLE II. Coarsening exponents for symmetric hopping.

Phase	Coarsening exponents
A	$\beta_1 = 1/3$
B	$\beta_2 = (1+\gamma)/(2+3\gamma)$
C, $\gamma \leqslant 1$	$\beta_1 = \beta_2 = 1/(2+\gamma)$
C, $\gamma > 1$	$\beta_1 = \beta_2 = 1/3$

in Fig. 5, where we get good data collapse on the symmetric time scale. The system sizes are, however, too small for a reasonable numeric estimate of the scaling exponent, but at least one can see that the exponent is significantly smaller than for totally asymmetric hopping (cf. Fig. 4 top).

For partially asymmetric hopping, excess particles return to the cluster site they just left with nonzero probability, but also the probability of reaching the next cluster site in the direction of the drive is of order 1, even in the limit $L \to \infty$. So in contrast to symmetric hopping, the coarsening time scale is only corrected by a constant factor independent of L, and the coarsening exponent is the same as in the totally asymmetric case.

It is interesting to compare our prediction for the exponents in phase B with the results of [18] and [19], in which the authors study a single-species zero-range process where the hop rates, $w_1, \ldots, w_L$, are site-dependent but independent of the particle occupation number at the departure site. They consider symmetric [18] and asymmetric [19] dynamics, where the (quenched) hop rates are drawn independently from a distribution $p(w)$ which can be written in the form

$$p(w) = [(\gamma^{-1}+1)/(1-\alpha)^{\gamma^{-1}+1}](w-\alpha)^{\gamma^{-1}}, \qquad (28)$$

where $w \in [\alpha, 1]$ with $\gamma, \alpha > 0$. This model undergoes a condensation transition above a critical particle density from a homogeneous phase to a phase with a condensate which resides at the site with the smallest hop rate. In both asymmetric and symmetric cases, they obtain coarsening exponents identical to those we obtain for the coarsening of the species 2 particles in phase B. One can think of the dynamics defined in Eq. (5) as a model of particles (species 2 particles) moving on an evolving disordered background (given by the species 1 particles). By the time the coarsening regime has been reached, at the cluster sites the evolving disorder is effectively quenched. Therefore, it is not necessarily surprising that the two models exhibit similar coarsening behavior for some distribution $p(w)$. The reason the form (28) is the relevant one for the rates (5) is as follows. In the disordered model, the coarsening is governed by the exchange of particles between the two slowest sites in the system. The rate at which particles are transferred between these two slowest sites is given by the difference between the two rates at these sites, Δw. For the distribution (28), $\Delta w \sim L^{-\gamma/(1+\gamma)}$. This rate separation contributes the same factor to the coarsening time scale as that in the two-species model due to the dependence of the hop rate of species 2 particles on the background of species 1 particles [see Eq. (22)]. The remaining contributions to the coarsening time scale are then determined by the symmetry of the hopping dynamics, i.e., the coarsening time scale is given by a factor of order L for asymmetric dynamics, or a factor of order L^2 for symmetric dynamics, multiplied by the inverse rate separation. This leads to the same exponents as those obtained for phase B.

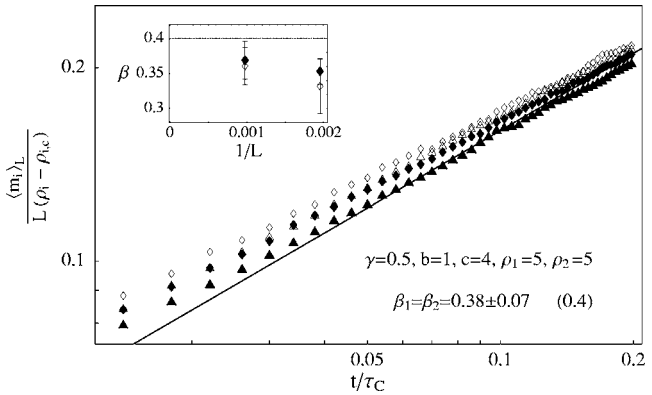

FIG. 5. Verification of the predicted scaling laws for symmetric hopping in phase C with $\gamma = 0.5$. Details of the plot are given in the caption to Fig. 3. Symbols $L = 512$ ($\diamond$) and 1024 ($\triangle$) for species 2 and filled symbols for species 1.

V. CONCLUSION

We have considered a two-species zero-range process which undergoes a variety of transitions to different condensate phases. The combination of two conservation laws and the coupling in the dynamics between the two species of particles leads to coarsening dynamics which are very rich compared to the single-species model. In particular, we have considered a case in which the dynamics of one of the particle species (the species 2 particles) depends only on the number of particles of the other species (species 1) at the departure site, and decays to a constant value as a power law with exponent γ. While the stationary phase diagram discussed in Sec. II B depends also on other system parameters, the coarsening exponents only depend (continuously) on γ and differ from phase to phase. Further, as expected, the exponents depend on the symmetry of the hopping dynamics.

ACKNOWLEDGMENTS

The authors thank the Max Planck Institute for Complex Systems, Dresden, where this work was initiated, for hospitality. T.H. was supported by EPSRC programme Grant No. GR/S10377/01.

APPENDIX: DISCUSSION OF FINITE-SIZE EFFECTS

In the following, we discuss qualitatively the most basic mechanisms leading to finite-size effects and illustrate how they depend on the system parameters. We start with two competing effects which influence the bulk density of the condensing species, connected with the definition of cluster sites by a threshold. (i) Excess particles exchanged between cluster sites increase the bulk density in finite systems. In phase B, for example, this effect is of order $L^{1-\gamma/(1+\gamma)}$

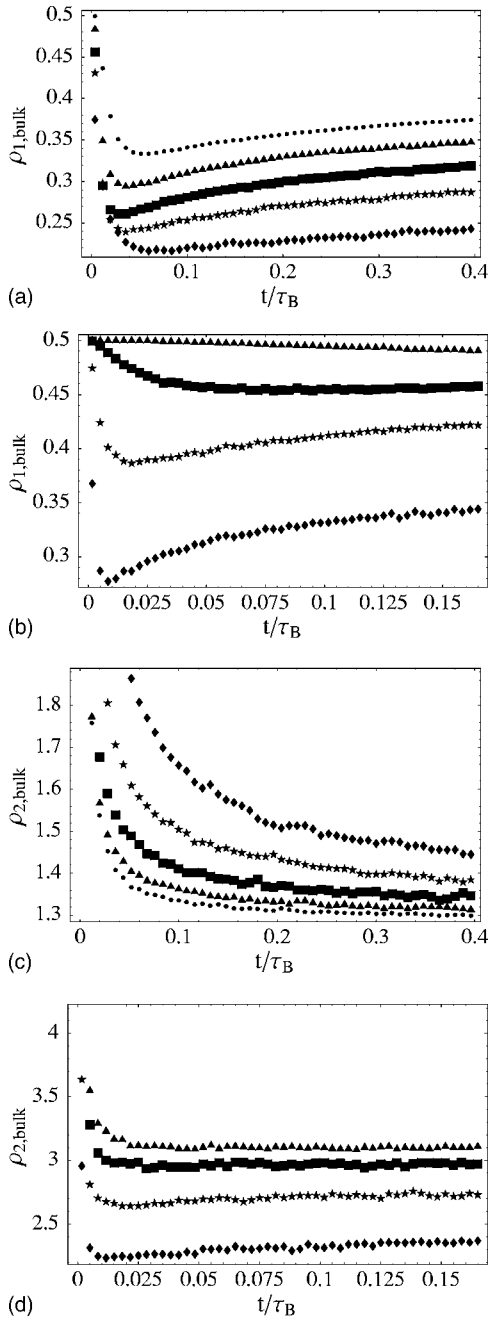

FIG. 6. Finite-size effects in phase B. $\rho_{1,\mathrm{bulk}}$ shown on the top is smaller than its limiting value $\rho_1=0.5$ for $L\to\infty$ since on species 2 cluster sites $k_1\sim L^{1/(1+\gamma)}$. With increasing γ this effect becomes weaker. $\rho_{2,\mathrm{bulk}}$ shown on the bottom converges to its limiting value $\rho_{2,c}$ from above (for $\gamma<1$) and from below (for $\gamma>1$) as explained in the text. (a), (c) $\gamma=0.7$, $b=1$, $c=3$, $\rho_1=0.5$, $\rho_2=5$, critical density $\rho_{2,c}=1.28$. Symbols: $L=256$ (♦), 512 (★), 1024 (■), 2048 (▲), and 4096 (●). (b), (d) $\gamma=2$, $b=1$, $c=4$, $\rho_1=0.5$, $\rho_2=10$, critical density $\rho_{2,c}=3.40$. Symbols: $L=256$ (♦), 512 (★), 1024 (■), and 2048 (▲).

$=L^{1/(1+\gamma)}$, by the reasoning given in Sec. III B and the expansion (22). It decreases with increasing γ and leads to a decrease of the mean condensate size. This effect is shown for $\gamma<1$ in Fig. 6(c), where $\rho_{2,\mathrm{bulk}}$ is plotted, decreasing toward $\rho_{2,c}$ with increasing system size L. (ii) On the other hand, bulk fluctuations increase with γ and in finite systems they can exceed the threshold for cluster sites. This leads to an increase of the number of condensed particles, or a decrease of $\rho_{2,\mathrm{bulk}}$, which dominates over effect (i) for $\gamma>1$. This can be seen in Fig. 6(d), where $\rho_{2,\mathrm{bulk}}$ now increases toward $\rho_{2,c}$. Since these fluctuations are typically small compared to other cluster sites, this leads also to a decrease of the mean condensate size. (iii) Further, in finite systems the nucleation and the coarsening regime are not clearly separated but overlap to a large extent, as can also be seen in Figs. 6(c) and 6(d). Ongoing nucleation effectively slows down the coarsening, leading to a decrease of the coarsening exponents for finite system sizes, as can be seen in the insets of Figs. 3 (bottom) and 4 (top).

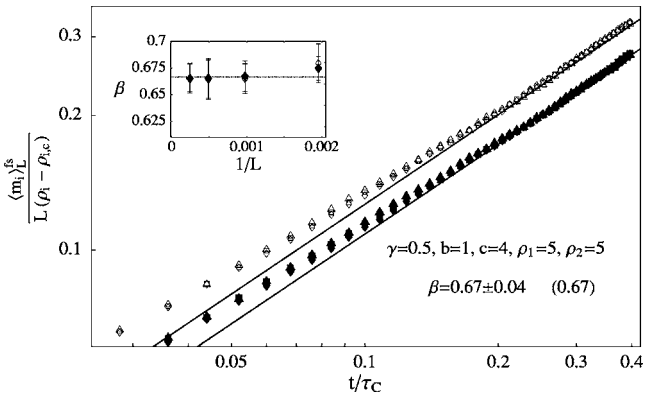

FIG. 7. Finite-size corrected data for phase C with $\gamma=0.5$ as given in Eq. (A2).

On top of these corrections, which are also present in single-species models, there are mechanisms specific to two-component systems. (iv) The coarsening dynamics does not only depend on the occupation number of the condensing species, but on the relation between k_1 and k_2. As discussed above, condensates with different relations have different lifetime. So in the limit $L\to\infty$, ratios differing by some factor L^α are dynamically separated and only one relation dominates the coarsening. But for finite systems, ratios with shorter lifetimes also contribute to the observed behavior. Thus data for single species systems, where this effect does not occur, are generically better than our data (cf. [2]). (v) Finally, we consider a phenomenon specific for phase B. As discussed above, on species 2 cluster sites there are of order $L^{1/(1+\gamma)}$ species 1 particles due to compatibility with the bulk. For $\gamma<1$, this is larger than a typical bulk fluctuation of order $L^{1/2}$, and reduces the bulk density of species 1 particles, whereas for $\gamma>1$ the effect is much weaker. This can be seen in Fig. 6 (top), where $\rho_{1,\mathrm{bulk}}$ is plotted.

The variety of effects leads to a diverse behavior, and a quantitative prediction of the finite-size corrections seems not to be feasible. However, it is straightforward to numerically fit the leading-order corrections for the prefactor and the exponent of the scaling law (9) using the ansatz

$$\frac{\langle m_i(t)\rangle_L}{(\rho_i-\rho_{i,c})L}=C_1(1+C_2/L^{\delta_1})\left(\frac{t}{\tau}\right)^{\beta_i+C_3/L^{\delta_2}}. \qquad \text{(A1)}$$

Consider, for instance, the data in phase C with $\gamma=0.5$ given in Fig. 4 (top). The finite-size corrections in the inset suggest

$\delta_2=1$ and the best-fit values for the other parameters are $\delta_1=0.69$, $C_1=0.51$, $C_2=2.3$, and $C_3=-21$ for species 1 and $\delta_1=0.60$, $C_1=0.59$, $C_2=2.1$, and $C_3=-13$ for species 2. In Fig. 7, we plot the corrected data

$$\frac{\langle m_i(t)\rangle_L^{fs}}{(\rho_i-\rho_{i,c})L}=\frac{\langle m_i(t)\rangle_L}{(\rho_i-\rho_{i,c})L}\left(\frac{t}{\tau}\right)^{-C_3/L^{\delta_2}}(C_1+C_2/L^{\delta_1})^{-1}, \tag{A2}$$

and the data collapse improves drastically.

[1] M. R. Evans, Braz. J. Phys. **30**, 42 (2000).
[2] S. Großkinsky, G. M. Schütz, and H. Spohn, J. Stat. Phys. **113**, 389 (2003).
[3] C. Godrèche, J. Phys. A **36**, 6313 (2003).
[4] Y. Kafri, E. Levine, D. Mukamel, G. M. Schütz, and J. Török, Phys. Rev. Lett. **89**, 035702 (2002).
[5] M. R. Evans, E. Levine, P. K. Mohanty, and D. Mukamel, Eur. Phys. J. B **41**, 223 (2004).
[6] J. D. Noh, G. M. Shim, and H. Lee, e-print cond-mat/0409120.
[7] A. G. Angel, M. R. Evans, and D. Mukamel, J. Stat. Mech.: Theor. Exp. , P04001 (2004).
[8] O. Pulkkinen and J. Merikoski, e-print cond-mat/0411630.
[9] M. R. Evans and T. Hanney, J. Phys. A **36**, L441 (2003).
[10] T. Hanney and M. R. Evans, Phys. Rev. E **69**, 016107 (2004).
[11] G. M. Schütz, J. Phys. A **36**, R339 (2003).
[12] R. Mikkelsen, D. van der Meer, K. van der Weele, and D. Lohse, Phys. Rev. Lett. **89**, 214301 (2002).
[13] S. N. Dorogovtsev, J. F. F. Mendes, and A. N. Samukhin, Nucl. Phys. B **666**, 396 (2003).
[14] S. Großkinsky and H. Spohn, Bull. Braz. Math. Soc. N. S. **34**, 1 (2003).
[15] S. Großkinsky (unpublished).
[16] A. J. Bray, Adv. Phys. **43**, 357 (1994); **51**, 481 (2002) (reprint).
[17] G. H. Weiss, *Aspects and Applications of the Random Walk* (North-Holland, Amsterdam, 1994).
[18] M. Barma and K. Jain, Pramana, J. Phys. **58**, 409 (2002).
[19] K. Jain and M. Barma, Phys. Rev. Lett. **91**, 135701 (2003).